


Article

High-Temperature Nano-Indentation Creep Behavior of Multi-Principal Element Alloys under Static and Dynamic Loads

Maryam Sadeghilaridjani and Sundeep Mukherjee * 

Department of Materials Science and Engineering, University of North Texas, Denton, TX 76203, USA; Maryam.Sadeghilaridjani@unt.edu

* Correspondence: sundeep.mukherjee@unt.edu; Tel.: +1-940-565-4170; Fax: 1-940-565-2944

Received: 14 January 2020; Accepted: 9 February 2020; Published: 13 February 2020



Abstract: Creep is a serious concern reducing the efficiency and service life of components in various structural applications. Multi-principal element alloys are attractive as a new generation of structural materials due to their desirable elevated temperature mechanical properties. Here, time-dependent plastic deformation behavior of two multi-principal element alloys, CoCrNi and CoCrFeMnNi, was investigated using nano-indentation technique over the temperature range of 298 K to 573 K under static and dynamic loads with applied load up to 1000 mN. The stress exponent was determined to be in the range of 15 to 135 indicating dislocation creep as the dominant mechanism. The activation volume was $\sim 25b^3$ for both CoCrNi and CoCrFeMnNi alloys, which is in the range indicating dislocation glide. The stress exponent increased with increasing indentation depth due to higher density and entanglement of dislocations, and decreased with increasing temperature owing to thermally activated dislocations. The results for the two multi-principal element alloys were compared with pure Ni. CoCrNi showed the smallest creep displacement and the highest activation energy among the three systems studied indicating its superior creep resistance.

Keywords: multi-principal element alloys; creep; nano-indentation; stress exponent; activation volume; activation energy

1. Introduction

Material degradation related to creep is a serious concern reducing the efficiency and service life of components in different structural applications. Therefore, there is strong demand for materials with inherently high creep resistance. Multi-principal element alloys (MPEAs) have attracted much attention as a new generation of structural materials with excellent mechanical properties including creep resistance [1–3]. MPEAs are composed of several elements in equiatomic or near-equiatomic proportion and despite complex chemistry, they usually form a simple single- or multi-phase solid solution [1–3]. The presence of different sized atoms in the unit cell leads to high degree of lattice strain in MPEAs [1] and results in high hardness and strength, good fracture toughness at cryogenic and elevated temperatures, high fatigue resistance, good wear, erosion and corrosion resistance [3–7]. Local lattice distortion, nano-clustering, and inhomogeneity at microstructural length scale in MPEAs [8] may significantly affect their mechanical properties including creep resistance. Therefore, probing the small-scale deformation behavior and local creep processes in MPEAs is critical in establishing their application worthiness. Nano-indentation technique has been widely used to characterize the small-scale deformation behavior of materials [9–15]. However, there are limited reports on the creep behavior of MPEAs using nano-indentation, and majority of the studies are at room temperature with a maximum load of 100 mN [16–22]. There are no reports on the deformation behavior of MPEAs as

a function of temperature comparing static and dynamic loads. This is important in wide ranging applications where components are subject to both static and cyclic loads such as aerospace, nuclear, automotive, and oil and gas industries [12].

Here, we report the nano-indentation creep behavior of two MPEAs, namely CoCrNi and CoCrFeMnNi. These were chosen as model alloys with excellent mechanical properties [23] and a single-phase face centered cubic (FCC) microstructure [10,24]. Nano-indentation creep was studied under static and dynamic loads as a function of temperature and peak load. Stress exponent, activation volume, and activation energy of the alloys were evaluated. Nickel (Ni) was used as the reference metal with FCC crystal structure for comparison with the two MPEAs.

2. Experimental

Alloys with nominal compositions of CoCrNi and CoCrFeMnNi in equimolar ratios were prepared by arc-melting high purity elements (>99.9%) in a Ti-gettered argon atmosphere. To ensure chemical homogeneity, the ingots were flipped and remelted several times. As-cast alloys and Ni were then rolled up to 70% reduction in thickness followed by annealing at 1173 K for 20 h to get equiaxed grains with low dislocation density. The annealed samples were polished with silicon carbide papers followed by diamond suspension to a mirror finish for microstructural characterization and nano-mechanical tests. Rigaku III Ultima X-ray diffractometer (XRD, Rigaku Corporation, Tokyo, Japan) with 1.54 Å wavelength Cu-K α radiation was used for crystal structure and phase characterization of the alloys. Microstructure, grain size, and grain orientation of the alloys were characterized by scanning electron microscopy (SEM) using FEI Quanta ESEM (FEI Company, Hillsboro, OR, USA) and electron backscatter diffraction (EBSD) technique.

Nano-indentation creep tests were done using a TI Premier Triboindenter (Bruker, Minneapolis, MN, USA) equipped with XSol600 heating stage for heating the samples up to 600 °C. To avoid oxidation, the tests were performed in a mixture of Ar + 5% H₂ gas environment. A Berkovich sapphire tip was used in all creep tests. The initial tip calibration was done with a standard fused quartz reference sample. For each material, we adopted two different types of tests: (i) static constant load and (ii) dynamic mechanical analyze (DMA). The static creep tests were done by ramping the load to 500 mN and 1000 mN at temperatures of 298 K, 423 K, and 573 K and then held at maximum load for 120 s to determine creep response followed by unloading. The aim was to compare creep performance of the selected alloys as a function of temperature at two different loads. High load was used for the static creep tests to minimize the effect of surface and avoid indentation size effect (ISE). In nano-DMA tests, the selected loads were 50 mN, 100 mN, 500 mN and 1000 mN to study the ISE on dynamic creep behavior at the two temperatures of 298 K and 423 K. The frequency and amplitude were set to 100 Hz and 10% of the peak load, respectively. In all tests, a high loading rate of 20 mN/s was chosen to minimize plastic deformation during the loading segment so creep primarily occurred during the dwell time. Prior to each creep test at elevated temperature, the sample was held at the prescribed set point for at least 20 min for temperature stabilization and the indenter tip was maintained close to the sample to reduce temperature gradient. The thermal drift was automatically corrected by the Triboindenter software and was between 0.05–0.1 nm/s during testing. The effect of drift was also minimized by using large indentation depth and a short hold time [25]. At least 16 indents were done for each condition and the distance between each indent was larger than 100 μ m to avoid interaction of their plastic zones.

3. Results

Figure 1 summarizes the microstructural characterization for CoCrNi, CoCrFeMnNi, and pure Ni. The backscattered SEM images of the homogenized samples are shown in Figure 1a,c,e with the insets showing X-ray diffraction patterns for the alloys. All the alloys showed single-phase FCC crystal structure without any secondary phases or precipitates. Figure 1b,d,f show the EBSD images of CoCrNi, CoCrFeMnNi, and Ni, respectively, indicating that all the alloys had equiaxed grains with the inset

showing the grain size distribution. The grain sizes for CoCrNi were in the range of 5–50 μm (average $\approx 19 \mu\text{m}$) and that for CoCrFeMnNi were in the range of 5–55 μm (average $\approx 22 \mu\text{m}$). Ni showed a grain size distribution of 5–65 μm with an average of 30 μm . Significant numbers of annealing twins were observed in the microstructures indicating low stacking fault energy in the MPEAs.

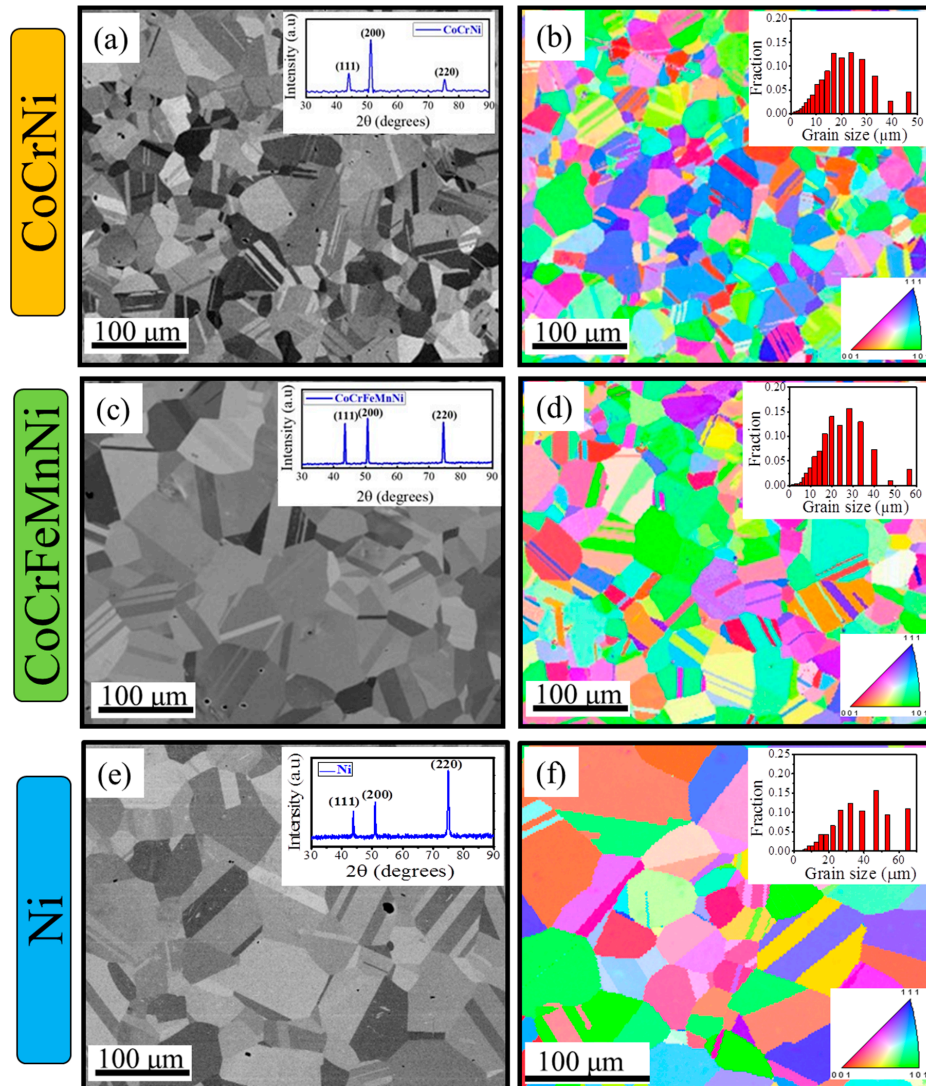


Figure 1. Backscattered SEM images with XRD patterns as insets for (a) CoCrNi, (c) CoCrFeMnNi, and (e) pure Ni. EBSD maps with grain size distribution as insets for (b) CoCrNi, (d) CoCrFeMnNi, and (f) pure Ni.

Creep behavior under static load was evaluated as a function of temperature at two different loads. The load and displacement data recorded during nano-indentation creep of CoCrFeMnNi MPEA is shown in Figure 2a,b as a function of temperature. Figure 2a shows the results at 500 mN load while Figure 2b shows the data at 1000 mN. For each test, an array of 4×4 indents was made with 100 μm distance between each indent, therefore covering grains with several different orientations. The plots for Ni and CoCrNi were very similar and not included here. At the same load, indentation depth in CoCrFeMnNi sample increased with increasing temperature from 298 K to 423 K, indicating reduction in hardness. The corresponding change in displacement during hold time was used to analyze the time-dependent deformation behavior of the alloys. This is plotted in Figure 2c,d for CoCrFeMnNi at temperatures of 298 K, 423 K, and 573 K and peak load of 500 mN and 1000 mN, respectively. The creep displacement increased rapidly with time in the beginning followed by slowing down of the rate of

increase. Fitting of the experimental data using an empirical relation for creep displacement is shown and elaborated later in the discussion section. Figure 2e,f show the magnitude of creep displacement as a function of temperature for Ni, CoCrNi, and CoCrFeMnNi alloys at the loads of 500 mN and 1000 mN, respectively. The maximum creep displacements were in the range of 50 nm to 400 nm, depending on the alloy, holding load, and temperature. Each data point in Figure 2e,f is the average of at least 16 indents with the error bar including possible influence of crystal orientation. Increase in temperature and peak load increased creep displacement for pure Ni since it is a thermally activated process and diffusion is enhanced at elevated temperature and high load. However, for the MPEAs, distinctly different behavior was seen compared to pure Ni. At 500 mN load, the creep displacement in the case of CoCrNi first increased from 298 K to 423 K and then decreased with further increase of temperature to 573 K. For CoCrFeMnNi, the creep displacement decreased with increasing temperature. This may be attributed to generation of partial dislocations at these intermediate temperatures and/or solute drag effects which restrict dislocation mobility [26–28]. Overall, CoCrNi showed the smallest creep displacement among the three systems for the load and temperature range investigated.

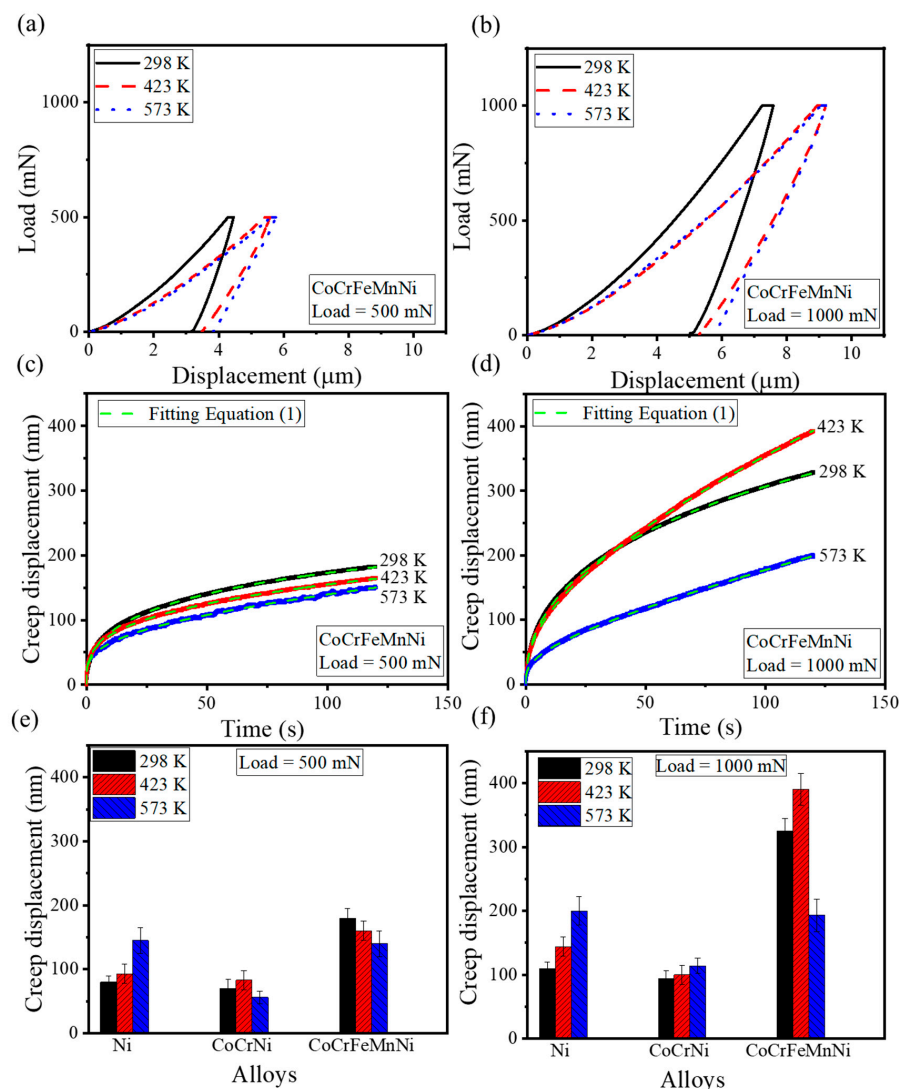


Figure 2. Typical load-displacement plot after nano-indentation creep tests for CoCrFeMnNi alloy as a function of temperature under applied load of (a) 500 mN and (b) 1000 mN. Creep displacement versus hold time for CoCrFeMnNi alloy at different temperatures under load of (c) 500 mN and (d) 1000 mN. Total creep displacement as a function of temperature for Ni, CoCrNi, and CoCrFeMnNi alloys at (e) 500 mN and (f) 1000 mN.

The local time-dependent plastic deformation of CoCrNi and CoCrFeMnNi MPEAs was studied under dynamic load and compared with pure Ni. The samples were loaded to 50 mN, 100 mN, 500 mN, and 1000 mN and held for 120 s under dynamic loads. In each test, the amplitude of load was fixed at 10% of the peak load. Figure 3a,b show the representative creep displacement versus holding time at various loads for CoCrFeMnNi at 298 K and 423 K. The maximum creep depth increased with increasing load from 50 mN to 1000 mN with similar behavior observed for Ni and CoCrNi. Figure 3c,d show the magnitude of maximum creep displacement as a function of load for all studied alloys at 298 K and 423 K. Increasing peak load led to increase in creep displacement due to dislocation activation. Total creep displacement was found to be in the order of CoCrNi < Ni < CoCrFeMnNi, which was in agreement with the data obtained from static loading. The effect of surface oxidation on the measured creep displacement is expected to be minimal due to the use of Ar + 5% H₂ gas environment and higher loads. There was no change in surface appearance of the samples after the high-temperature tests indicating minimal oxidation.

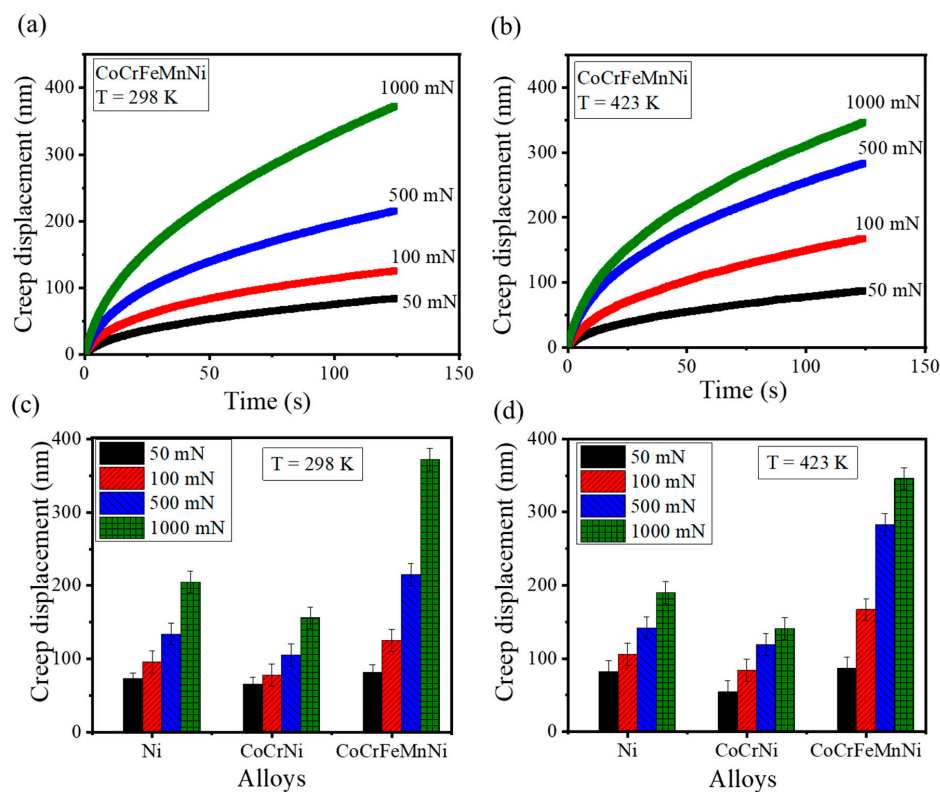


Figure 3. Representative creep displacement versus hold time for CoCrFeMnNi alloy as a function of loads at (a) 298 K and (b) 423 K. Maximum creep displacement for the three alloys at (c) 298 K and (d) 423 K showing larger creep depth with increase in load.

4. Discussion

Creep displacement, h , is a function of time, t , and follows the empirical relation [18]:

$$h(t) = h_0 + a(t - t_0)^p + kt \quad (1)$$

where h_0 and t_0 are the initial depth and time during creep period and a , p , and k are fitting constants. The dashed lines in Figure 2c,d represent the fitting curves corresponding to Equation (1) with

correlation coefficient $R^2 > 0.95$. For self-similar indentation probe similar to Berkovich used in the current study, indentation strain rate ($\dot{\epsilon}$) and hardness (H) were obtained as [18]:

$$\dot{\epsilon} = \frac{1}{h} \frac{dh}{dt} \quad (2)$$

and

$$H = \frac{P}{24.5h_c^2} \quad (3)$$

where $\frac{dh}{dt}$ is the first derivative of the displacement-time curve (i.e., Equation (1)) with respect to t , P is applied load, h_c is contact depth given by $h_c = h_{\max} - 0.75P/S$ for Berkovich indenter, and h_{\max} and S are maximum penetration depth and material stiffness, respectively. The hardness measured from Equation (3) was divided by 0.9 for sink-in and 1.02 for pile-up [29,30]. The susceptibility for pile-up or sink-in in nano-indentation tests can be found by the ratio of final indentation depth to the maximum indentation depth (h_f/h_{\max}) with $h_f/h_{\max} \geq 0.7$ indicating pile-up and $h_f/h_{\max} < 0.7$ indicating sink-in [31]. Since plastic deformation is a thermally activated process, stress exponent (reciprocal of strain rate sensitivity) provides valuable insight into creep deformation mechanism [18]. The creep stress exponent was calculated for the two MPEAs and pure Ni and its dependence on load and temperature was evaluated.

The creep stress exponent (denoted by n) was calculated from the slope of $\ln \dot{\epsilon}$ versus $\ln H$ curves [18]. Figure 4 shows the creep stress exponent for the two MPEAs and pure Ni under static load to evaluate the effect of temperature and under dynamic (DMA) mode to study the effect of peak load or indentation depth. Static test analysis was done at two different loads of 500 mN and 1000 mN as shown in Figure 4a,b, respectively. Dynamic test analysis was done at two different temperatures of 298 K and 423 K as shown in Figure 4c,d, respectively. The n value for each condition was obtained from an average of 16 independent indentations. The average n values for the three systems were in the range of 15 to 135 in static tests. Creep stress exponent defines the creep mechanism. Typically, $n = 1$ is associated with diffusion creep (by lattice or grain boundary diffusion), $n = 2$ with grain boundary sliding, and $n > 3$ with dislocation creep [23]. Therefore, for all the current alloys, deformation was dominated by dislocation creep (climb or glide). The stress exponent for Ni dropped from 135 at 298 K to 50–60 at 573 K, likely due to thermally activated dislocations at elevated temperature. In a similar study, the stress exponent was found to be in the range of 20–60 for IN-718 at room temperature and decreased to 8–18 at 923 K [32]. The magnitude of stress exponent depends on the balance between generation and annihilation of dislocations [33]. Larger value of stress exponent is typically obtained when more dislocations are generated and involved during deformation [33]. The decrease in n value with increasing temperature may be due to enhancement in dislocation diffusivity and thermal recovery at higher temperature, so annihilation competes with dislocation generation. The negligible change in stress exponent as a function of temperature for CoCrFeMnNi HEA may be attributed to dislocation glide dictated deformation, which is thermally insensitive [34]. Since glide does not require interatomic diffusion (unlike climb), it is the dominant mechanism of deformation even at low temperature and is thermally insensitive [34]. Transmission electron microscopy (TEM) studies of MPEAs showed that in the early stages of plastic deformation, glide of dislocations on {111} planes was the dominant mechanism [35]. Due to low stacking fault energy and partial dislocations in MPEAs, cross slip is hindered, and plasticity occurs by dislocation glide [35]. The temperature independent stress exponent for CoCrFeMnNi may be attributed to sluggish diffusion [1,2], which would favor glide over climb dominated deformation. For pure Ni, deformation was climb dominated over the temperature range studied. For CoCrNi, the sharp drop in creep stress exponent is likely from change in climb dominated creep at low temperatures (similar to pure Ni) to glide dominated creep at high temperatures (similar to CoCrFeMnNi). In summary, the stress exponent for CoCrNi was close to that of pure Ni at room temperature but became similar to CoCrFeMnNi MPEA at the higher temperature. Recent atomistic modeling suggests that the CoCrNi system shows partial chemical ordering at the atomic scale at

room temperature while becoming random solid solution at higher temperatures [36]. Partial local ordering may act as barrier for dislocation movement explaining the much higher stress exponent for CoCrNi at 298 K compared to CoCrFeMnNi. Figure 4c,d show the variation in stress exponent for the dynamic tests. As the peak load increased from 50 mN to 1000 mN, the n value increased at both the temperatures of 298 K and 423 K, which is attributed to ISE [37,38]. During the loading process, dislocations are generated in the plastic deformation region beneath the indenter and their density is directly proportional to the load or depth [39]. At low load, dislocation generation rate is slow, and the stress exponent is low. At high load, dislocation generation rate is fast, and they interact and entangle with one another leading to increase in the stress exponent with value up to 100 for pure Ni [19,40]. The observed ISE of n may also be related to the mobility and diffusion of dislocations and how far they are from the free surface [41]. At smaller depth, dislocations are closer to the free surface and therefore have higher mobility and diffusion leading to lower n .

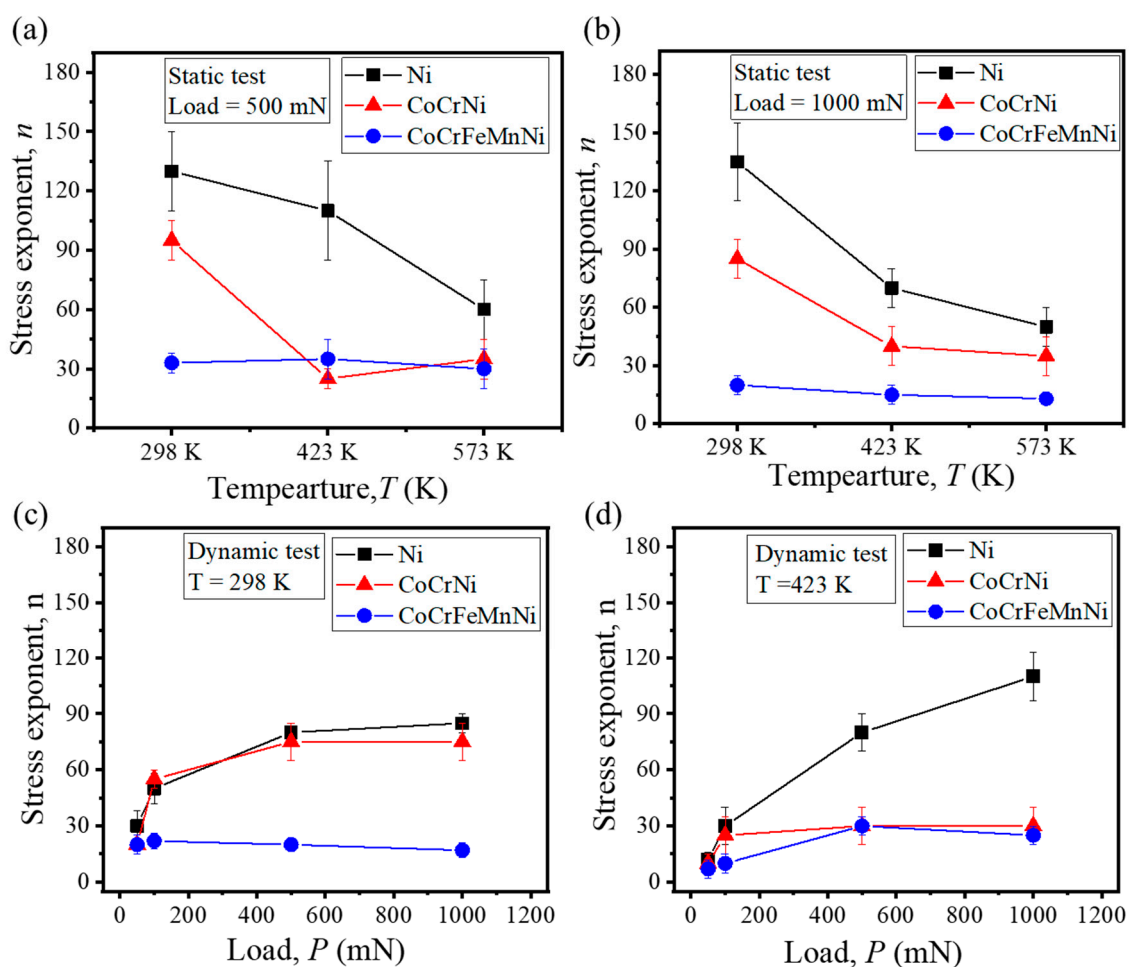


Figure 4. Stress exponent versus temperature from static test for Ni, CoCrNi and CoCrFeMnNi alloys at (a) 500 mN and (b) 1000 mN showing decrease of stress exponent with increasing temperature for Ni and negligible dependence of stress exponent on temperature for CoCrFeMnNi HEA. Stress exponent versus load from dynamic test for all alloys at (c) 298 K and (d) 423 K showing indentation size effect for stress exponent.

The high values of stress exponent obtained from nano-indentation of the three alloys may be attributed to the complex stress state underneath the indenter [16,21,38]. The stress exponent is a complex function of microstructure, mobile dislocation density and/or the activation area underneath the indenter [42]. The n value for Ni was significantly larger than those of MPEAs, even though the rate-controlling mechanism was the same for all three systems studied (i.e., dislocation dominated

deformation mechanism) with almost identical microstructure. From Figure 4, it was concluded that the stress exponent determined from dynamic tests was slightly lower than that in static test. This may be because of oscillatory load which resulted in better propagation of dislocations and reduction of n .

For further insight into the mechanism of creep, the activation volume (V^*) for the three systems was evaluated as [43]:

$$V^* = \frac{3 \cdot \sqrt{3} \cdot k \cdot T \cdot n}{H} \quad (4)$$

where k is Boltzmann constant, H is hardness, n is stress exponent and T is temperature. The activation volume depends on the stress exponent and hardness. The obtained activation volume for the three systems averaged over the three temperatures (298 K, 423 K, and 573 K) and two loads (500 mN and 1000 mN) were $2.2 \pm 0.1 \text{ nm}^3$ ($\sim 143b^3$), $0.4 \pm 0.11 \text{ nm}^3$ ($\sim 25b^3$) and $0.43 \pm 0.1 \text{ nm}^3$ ($\sim 26b^3$) for Ni, CoCrNi, and CoCrFeMnNi, respectively. Here, the Burgers vector (b) for the FCC alloys was calculated as $b = 1/2a_0$ [110], where a_0 is the lattice parameter with values of 0.352 nm, 0.3567 nm and 0.3597 nm for Ni, CoCrNi, and CoCrFeMnNi, respectively [35,44]. V^* in the range of $100b^3$ – $1000b^3$ is associated with dislocation interaction mechanism and in the range of $10b^3$ – $100b^3$ with dislocation glide [45]. Therefore, the obtained activation volume for Ni was in the range for dislocation interaction while the lower value of V^* for the two MPEAs indicates dislocation glide mechanism. Activation energy for dislocation nucleation is higher for a MPEA compared to pure metal [10]. Therefore, lower dislocation density in MPEAs favors dislocation glide over dislocation-dislocation interaction. In similar studies, CoCrFeMnNi homogenized sample showed activation volume of 0.2 – 1.02 nm^3 using stress relaxation tests in the temperature range of 873 K to 1073 K [46] and activation volume of $52b^3$ and $209b^3$ were reported for coarse grained Ni and Al from nano-indentation tests, respectively [11]. In addition, Ni-based superalloy (IN-718) showed activation volume in the range of 0.05 to 0.1 nm^3 within temperature range of 298 K to 923 K in tensile creep experiment [32].

The temperature dependence of indentation creep rate may be expressed as a power-law relation as [47]:

$$\dot{\epsilon} = A\sigma^n \exp\left(-\frac{Q}{RT}\right) \approx AH^n \exp\left(-\frac{Q}{RT}\right) \quad (5)$$

where A is a material constant, R is universal gas constant, and Q is the creep activation energy. The slope of $\ln(\dot{\epsilon}/H^n)$ versus $1/T$ curve gives the value of $-Q/R$ [48,49] as shown in Figure 5 for the three studied systems. The average strain rate and hardness at each temperature over the holding time was selected for analysis. The creep activation energy of Ni, CoCrNi, and CoCrFeMnNi were found to be $200 \pm 20 \text{ kJ/mol}$, $400 \pm 100 \text{ kJ/mol}$ and $25 \pm 5 \text{ kJ/mol}$, respectively. The creep activation energy of CoCrNi was estimated to be 400 kJ/mol , while that of creep resistant Ni-based superalloy such as CMSX-2 and IN-X750 calculated from uniaxial tensile test was 230 kJ/mol and 306 kJ/mol , respectively [50,51]. CoCrNi showed the lowest creep displacement and highest activation energy supporting its superior creep resistance. Hardness or strength has a pronounced effect on creep resistance as previously reported [16,18]. CoCrNi showed the highest hardness compared to the other two systems and thus better creep resistance. However, the hardness of Ni and CoCrFeMnNi were similar and we attributed the lower creep resistance of CoCrFeMnNi alloy to its lower stacking fault energy (SFE) compared to Ni [52]. In confined volume deformation as in nano-indentation, lower SFE may result in increased dislocation generation and plastic flow, thus reducing creep resistance during holding time [52].

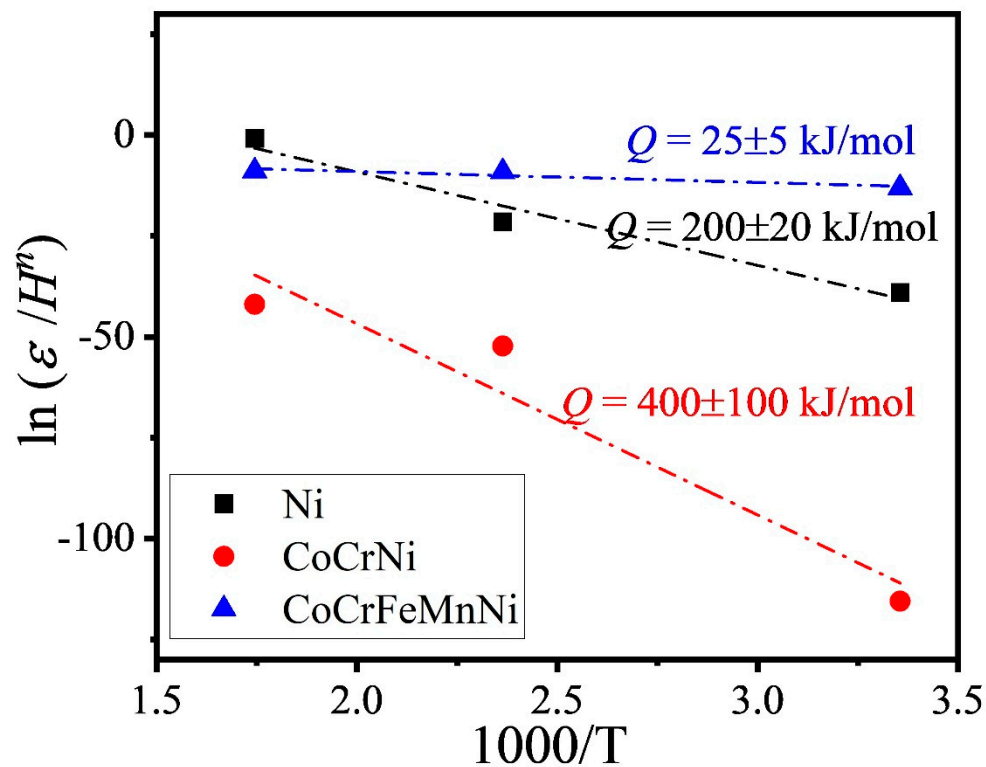


Figure 5. $\ln(\dot{\epsilon}/H^n)$ versus $1000/T$ with slope giving the activation energy (Q) for Ni, CoCrNi, and CoCrFeMnNi alloys.

5. Conclusions

In summary, nano-indentation creep tests for CoCrNi and CoCrFeMnNi MPEAs were performed under static and dynamic (DMA) loads at 298 K, 423 K, and 573 K. Stress exponent was calculated from steady-state creep. The creep behavior of the alloys was compared in terms of stress exponent, activation volume, and activation energy. The following conclusions may be drawn:

- (1) The value of n was in the range of 15 to 135 indicating that time-dependent deformation for all alloys was dislocation dominated.
- (2) Activation volume data suggested dislocation glide dominated deformation mechanism for MPEAs and dislocation-dislocation interaction for pure Ni.
- (3) The stress exponent decreased with increasing temperature due to thermally activated dislocations. The stress exponent for CoCrFeMnNi was found to be temperature insensitive possibly due to dislocation glide dominated deformation.
- (4) The creep stress exponent increased with increasing load (depth) due to higher generation rate of dislocations and their entanglement at greater depth.
- (5) CoCrNi showed creep behavior similar to pure Ni at room temperature while it became closer to CoCrFeMnNi at higher temperatures. This may be due to the local chemical ordering in CoCrNi at lower temperatures while becoming more random solid solution like at higher temperatures.

Author Contributions: Conceptualization, M.S. and S.M.; methodology, M.S.; validation, M.S. and S.M.; formal analysis, M.S.; investigation, M.S.; data curation, M.S. and S.M.; writing—original draft preparation, M.S.; writing—review and editing, S.M.; visualization, M.S. and S.M.; supervision, S.M.; Project administration, S.M.; All authors have read and agreed to the published version of the manuscript.

Funding: Sundeep Mukherjee acknowledges funding from the National Science Foundation (NSF) under Grant Number 1762545 (CMMI) for part of this work. Any opinions, findings, and conclusions expressed in this paper are those of the authors and do not necessarily reflect the views of the National Science Foundation (NSF).

Acknowledgments: The authors thank the Materials Research Facility (MRF) at University of North Texas for access to the characterization equipment used in this study.

Conflicts of Interest: The authors declare no conflict of interest.

References

1. Miracle, D.B.; Senkov, O.N. A critical review of high entropy alloys and related concepts. *Acta Mater.* **2017**, *122*, 448–511. [[CrossRef](#)]
2. Senkov, O.N.; Miracle, D.B.; Chaput, K.J.; Couzinié, J.-P. Development and exploration of refractory high entropy alloys—A review. *J. Mater. Res.* **2018**, *33*, 3092–3128. [[CrossRef](#)]
3. Zhang, Y.; Zuo, T.T.; Tang, Z.; Gao, M.C.; Dahmen, K.A.; Liaw, P.K.; Lu, Z.P. Microstructures and properties of high entropy alloys. *Prog. Mater. Sci.* **2014**, *61*, 1–93. [[CrossRef](#)]
4. Gludovatz, B.; Hohenwarter, A.; Thurston, K.V.; Bei, H.; Wu, Z.; George, E.P.; Ritchie, R.O. Exceptional damage-tolerance of a medium-entropy alloy CrCoNi at cryogenic temperatures. *Nat. Commun.* **2016**, *7*, 1–8. [[CrossRef](#)]
5. Gali, A.; George, E.P. Tensile properties of high-and medium-entropy alloys. *Intermetallics* **2013**, *39*, 74–78. [[CrossRef](#)]
6. Nair, R.B.; Arora, H.S.; Mukherjee, S.; Singh, S.; Singh, H.; Grewal, H.S. Exceptionally high cavitation erosion and corrosion resistance of a high entropy alloy. *Ultrason. Sonochem.* **2018**, *41*, 252–260. [[CrossRef](#)]
7. Ayyagari, A.; Hasannaemi, V.; Grewal, H.S.; Arora, H.; Mukherjee, S. Corrosion, erosion and wear behavior of complex concentrated alloys: A review. *Metals* **2018**, *8*, 603. [[CrossRef](#)]
8. Xu, X.D.; Liu, P.; Guo, S.; Hirata, A.; Fujita, T.; Nieh, T.G.; Liu, C.T.; Chen, M.W. Nanoscale phase separation in a fcc-based CoCrCuFeNiAl_{0.5} high-entropy alloy. *Acta Mater.* **2015**, *84*, 145–152. [[CrossRef](#)]
9. Sadeghilaridjani, M.; Mukherjee, S. Strain gradient plasticity in multiprincipal element alloys. *JOM* **2019**, *71*, 3466–3472. [[CrossRef](#)]
10. Mridha, S.; Sadeghilaridjani, M.; Mukherjee, S. Activation Volume and energy for dislocation nucleation in multi-principal element alloys. *Metals* **2019**, *9*, 263. [[CrossRef](#)]
11. Maier, V.; Merle, B.; Göken, M.; Durst, K. An improved long-term nanoindentation creep testing approach for studying the local deformation processes in nanocrystalline metals at room and elevated temperatures. *J. Mater. Res.* **2013**, *28*, 1177–1188. [[CrossRef](#)]
12. Sadeghilaridjani, M.; Ayyagari, A.; Muskeri, S.; Hasannaemi, V.; Salloom, R.; Chen, W.-Y.; Mukherjee, S. Ion irradiation response and mechanical behavior of reduced activity high entropy alloy. *J. Nucl. Mater.* **2020**, *529*, 151955. [[CrossRef](#)]
13. Sadeghilaridjani, M.; Muskeri, S.; Hasannaemi, V.; Pole, M.; Mukherjee, S. Strain rate sensitivity of a novel refractory high entropy alloy: Intrinsic versus extrinsic effects. *Mater. Sci. Eng. A* **2019**, *766*, 138326. [[CrossRef](#)]
14. Mridha, S.; Komarasamy, M.; Bhowmick, S.; Mishra, R.S.; Mukherjee, S. Small-scale plastic deformation of nanocrystalline high entropy alloy. *Entropy* **2018**, *20*, 889. [[CrossRef](#)]
15. Li, W.H.; Shin, K.; Lee, C.G.; Wei, B.C.; Zhang, T.H.; He, Y.Z. The characterization of creep and time-dependent properties of bulk metallic glasses using nanoindentation. *Mater. Sci. Eng. A* **2008**, *478*, 371–375. [[CrossRef](#)]
16. Ma, Y.; Feng, Y.H.; Debela, T.T.; Peng, G.J.; Zhang, T.H. Nanoindentation study on the creep characteristics of high-entropy alloy films: fcc versus bcc structures. *Int. J. Refract. Met. Hard Mater.* **2016**, *54*, 395–400. [[CrossRef](#)]
17. Lee, D.-H.; Seok, M.-Y.; Zhao, Y.; Choi, I.-C.; He, J.; Lu, Z.; Suh, J.-Y.; Ramamurty, U.; Kawasaki, M.; Langdon, T.G.; et al. Spherical nanoindentation creep behavior of nanocrystalline and coarse-grained CoCrFeMnNi high-entropy alloys. *Acta Mater.* **2016**, *109*, 314–322. [[CrossRef](#)]
18. Ma, Y.; Peng, G.J.; Wen, D.H.; Zhang, T.H. Nanoindentation creep behavior in a CoCrFeCuNi high-entropy alloy film with two different structure states. *Mater. Sci. Eng. A* **2015**, *621*, 111–117. [[CrossRef](#)]
19. Wang, Z.; Guo, S.; Wang, Q.; Liu, Z.; Wang, J.; Yang, Y.; Liu, C.T. Nanoindentation characterized initial creep behavior of a high-entropy-based alloy CoFeNi. *Intermetallics* **2014**, *53*, 183–186. [[CrossRef](#)]
20. Wang, X.; Gong, P.; Deng, L.; Jin, J.; Wang, S.; Zhou, P. Nanoindentation study on the room temperature creep characteristics of a senary Ti_{16.7}Zr_{16.7}Hf_{16.7}Cu_{16.7}Ni_{16.7}Be_{16.7} high entropy bulk metallic glass. *J. Non-Cryst. Solids* **2017**, *470*, 27–37. [[CrossRef](#)]

21. Zhang, L.; Yu, P.; Cheng, H.; Zhang, H.; Diao, H.; Shi, Y.; Chen, B.; Chen, P.; Feng, R.; Bai, J.; et al. Nanoindentation creep behavior of an Al_{0.3}CoCrFeNi high-entropy alloy. *Metall. Mater. Trans. A* **2016**, *47*, 5871–5875. [[CrossRef](#)]
22. Jiao, Z.-M.; Ma, S.-G.; Yuan, G.-Z.; Wang, Z.-H.; Yang, H.-J.; Qiao, J.-W. Plastic deformation of Al_{0.3}CoCrFeNi and AlCoCrFeNi high-entropy alloys under nanoindentation. *J. Mater. Eng. Perform.* **2015**, *24*, 3077–3083. [[CrossRef](#)]
23. Li, Z.; Zhao, S.; Ritchie, R.O.; Meyers, M.A. Mechanical properties of high-entropy alloys with emphasis on face-centered cubic alloys. *Prog. Mater. Sci.* **2019**, *102*, 296–345. [[CrossRef](#)]
24. Mridha, S.; Das, S.; Aouadi, S.; Mukherjee, S.; Mishra, R.S. Nanomechanical behavior of CoCrFeMnNi high-entropy alloy. *JOM* **2015**, *67*, 2296–2302. [[CrossRef](#)]
25. Wheeler, J.M.; Armstrong, D.E.J.; Heinz, W.; Schwaige, R. High temperature nanoindentation: The state of the art and future challenges. *Curr. Opin. Solid State Mater. Sci.* **2015**, *19*, 354–366. [[CrossRef](#)]
26. Tsao, T.-K.; Yeh, A.-C.; Kuo, C.-M.; Kakehi, K.; Murakami, H.; Yeh, J.-W.; Jian, S.-R. The high temperature tensile and creep behaviors of high entropy superalloy. *Sci. Rep.* **2017**, *7*, 12658. [[CrossRef](#)] [[PubMed](#)]
27. Kang, Y.B.; Shim, S.H.; Lee, K.H.; Hong, S.I. Dislocation creep behavior of CoCrFeMnNi high entropy alloy at intermediate temperatures. *Mater. Res. Lett.* **2018**, *6*, 689–695. [[CrossRef](#)]
28. Sawant, A.; Tin, S.; Zhao, J.-C. High Temperature Nano-Indentation of Ni-Based Superalloys. Proceeding of the 11th International Symposium on Superalloys, TMS (The Minerals, Metals & Materials Society), Champion, PA, USA, 14–17 September 2008; pp. 863–871.
29. Haghshenas, M.; Wang, Y.; Cheng, Y.-T.; Gupta, M. Indentation-based rate-dependent plastic deformation of polycrystalline pure magnesium. *Mater. Sci. Eng. A* **2018**, *716*, 63–71. [[CrossRef](#)]
30. McElhane, K.W.; Vlassak, J.J.; Nix, W.D. Determination of indenter tip geometry and indentation contact area for depth-sensing indentation experiments. *J. Mater. Res.* **1998**, *13*, 1300–1306. [[CrossRef](#)]
31. Chen, J.; Shen, Y.; Liu, W.; Beake, B.D.; Shi, X.; Wang, Z.; Zhang, Y.; Guo, X. Effects of loading rate on development of pile-up during indentation creep of polycrystalline copper. *J. Mater. Sci. A* **2016**, *656*, 216–221. [[CrossRef](#)]
32. Wang, H.; Dhiman, A.; Ostergaard, H.E.; Zhang, Y.; Siegmund, T.; Kruzic, J.J.; Tomar, V. Nanoindentation based properties of Inconel 718 at elevated temperatures: A comparison of conventional versus additively manufactured samples. *Int. J. Plast.* **2019**, *120*, 380–394. [[CrossRef](#)]
33. Zhang, W.-D.; Liu, Y.; Wu, H.; Lan, X.-D.; Qiu, J.; Hu, T.; Tang, H.-P. Room temperature creep behavior of Ti–Nb–Ta–Zr–O alloy. *Mater. Charact.* **2016**, *118*, 29–36. [[CrossRef](#)]
34. Morris Jr, J.W. Dislocation-controlled plasticity of crystalline materials: Overview. In *Encyclopedia of Materials: Science and Technology*, 2nd ed.; Elsevier: Amsterdam, The Netherlands, 2001; pp. 2245–2255.
35. Laplanche, G.; Kostka, A.; Reinhart, C.; Hunfeld, J.; Eggeler, G.; George, E.P. Reasons for the superior mechanical properties of medium-entropy CrCoNi compared to high-entropy CrMnFeCoNi. *Acta Mater.* **2017**, *128*, 292–303. [[CrossRef](#)]
36. Li, Q.-J.; Sheng, H.; Ma, E. Strengthening in multi-principal element alloys with local-chemical-order roughened dislocation pathways. *Nat. Commun.* **2019**, *10*, 3563. [[CrossRef](#)]
37. Nix, W.D.; Gao, H. Indentation size effects in crystalline materials: A law for strain gradient plasticity. *J. Mech. Phys. Solids* **1998**, *46*, 411–425. [[CrossRef](#)]
38. Li, H.; Ngan, A.H.W. Size effects of nanoindentation creep. *J. Mater. Res.* **2004**, *19*, 513–522. [[CrossRef](#)]
39. Almasri, A.H.; Voyiadjis, G.Z. Effect of strain rate on the dynamic hardness in metals. *J. Eng. Mater. Tech.* **2007**, *129*, 505–512. [[CrossRef](#)]
40. Liu, Y.; Huang, C.; Bei, H.; He, X.; Hu, W. Room temperature nanoindentation creep of nanocrystalline Cu and Cu alloys. *Mater. Lett.* **2012**, *70*, 26–29. [[CrossRef](#)]
41. Zhao, J.; Wang, F.; Huang, P.; Lu, T.J.; Xu, K.W. Depth dependent strain rate sensitivity and inverse indentation size effect of hardness in body-centered cubic nanocrystalline metals. *Mater. Sci. Eng. A* **2014**, *615*, 87–91. [[CrossRef](#)]
42. Oikawa, H.; Karashima, S. On the stress exponent and the rate-controlling mechanism of high-temperature creep in some solid solutions. *Metall. Trans.* **1974**, *5*, 1179–1182. [[CrossRef](#)]
43. Phani, P.S.; Oliver, W.C. A direct comparison of high temperature nanoindentation creep and uniaxial creep measurements for commercial purity aluminum. *Acta Mater.* **2016**, *111*, 31–38. [[CrossRef](#)]

44. Owen, L.R.; Pickering, E.J.; Playford, H.Y.; Stone, H.J.; Tucker, M.G.; Jones, N.G. An assessment of the lattice strain in the CrMnFeCoNi high-entropy alloy. *Acta Mater.* **2017**, *122*, 11–18. [[CrossRef](#)]
45. Monclús, M.A.; Molina-Aldareguia, J.M. High temperature nanomechanical testing. In *Handbook of Mechanics of Materials*; Hsueh, C.H., Schmauder, S., Chen, C.-S., Chawla, K.K., Chawla, N., Chen, W., Kagawa, Y., Eds.; Springer: Singapore, 2018.
46. He, J.Y.; Zhu, C.; Zhou, D.Q.; Liu, W.H.; Nieh, T.G.; Lu, Z.P. Steady state flow of the FeCoNiCrMn high entropy alloy at elevated temperatures. *Intermetallics* **2014**, *55*, 9–14. [[CrossRef](#)]
47. Li, Y.J.; Mueller, J.; Hoppel, H.W.; Goken, M.; Blum, W. Deformation kinetics of nanocrystalline nickel. *Acta Mater.* **2007**, *55*, 5708–5717. [[CrossRef](#)]
48. Shen, L.; Wu, Y.; Wang, S.; Chen, Z. Creep behavior of Sn–Bi solder alloys at elevated temperatures studied by nanoindentation. *J. Mater. Sci.: Mater. Electron.* **2017**, *28*, 4114–4124. [[CrossRef](#)]
49. Ginder, R.S.; Pharr, G.M. Characterization of power-law creep in the solid-acid CsHSO₄ via nanoindentation. *J. Mater. Res.* **2019**, *34*, 1130–1137. [[CrossRef](#)]
50. Rouault-Rogez, H.; Dupeux, M.; Ignat, M. High temperature tensile creep of CMSX-2 Nickel base superalloy single crystals. *Acta Metall. Mater.* **1994**, *42*, 3137–3148. [[CrossRef](#)]
51. Picasso, A.C.; Marzocca, A.J. On apparent activation energies of creep in nickel-base superalloys. *Scrp. Mater.* **1999**, *41*, 797–802. [[CrossRef](#)]
52. Hu, J.; Sun, G.; Zhang, X.; Wang, G.; Jiang, Z.; Han, S.; Zhang, J.; Lian, J. Effects of loading strain rate and stacking fault energy on nanoindentation creep behaviors of nanocrystalline Cu, Ni-20 wt. %Fe and Ni. *J. Alloys Compd.* **2015**, *647*, 670–680. [[CrossRef](#)]



© 2020 by the authors. Licensee MDPI, Basel, Switzerland. This article is an open access article distributed under the terms and conditions of the Creative Commons Attribution (CC BY) license (<http://creativecommons.org/licenses/by/4.0/>).